Magnetoelectric Néel anisotropies

Ralph Skomski*
Max-Planck-Institut für Mikrostrukturphysik, Weinberg 2, 06120 Halle, Germany
Present address: Department of Physics and Astronomy, University of Nebraska, Lincoln, NE 68588-0111

Abstract — **The applicability of Néel's pair model to metallic 3d surfaces and interfaces is explained in terms of the tight-binding moments-theorem. The Néel model reproduces itinerant magnetism so long as the band structure is approximated by third-moment atomic-pair contributions. This establishes an atomic Néel description of interfaces and impurities. The Néel parameter g depends on the d-band filling and, to some extent, on the atomic structure.**

Index terms — **anisotropy, itinerant magnetism**

I. Introduction

Since Néels pioneering work on magnetic surface anisotropy [1], the expansion of pair anisotropy energies into Legendre polynomials has become a widely-used tool in thin-film and surface magnetism. This refers in particular to complicated structures and morphologies such as ultrathin transition-metal films [2], multilayers [3], rough surfaces [4], [5], and surface steps [5], [6], where first-principle calculations are difficult to perform.

In lowest order, the Néel energy of a pair of magnetic atoms located at $\mathbf{R}_i$ and $\mathbf{R}_j$ is

$$E_{ij} = \frac{g(|\mathbf{R}|)}{2}(3\cos^2\alpha_{ij} - 1) \qquad (1)$$

Here α_{ij} is the angle between the common magnetization direction and $\mathbf{R} = \mathbf{R}_i - \mathbf{R}_j$, and g is a coupling constant. For example, the magnetostatic pair interaction

$$E_{ij} = -\frac{\mu_0}{4\pi}\frac{3\,\mathbf{m}_i.\mathbf{R}\;\mathbf{m}_j.\mathbf{R} - \mathbf{m}_i.\mathbf{m}_j\;R^2}{R^5} \qquad (2)$$

where $m = |\mathbf{m}_i|$ is the moment of the interacting dipoles, yields $g = -\mu_0 m^2/2\pi R^3$.

As early as 1931, Bloch and Gentile [7] recognized that magnetic anisotropy does not reflect magnetostatic interactions but is caused by largely atomic spin-orbit and electrostatic crystal-field interactions. Here we will use the name *magnetoelectric* rather than magnetocrystalline, because the mechanism is not restricted to crystals. Note that Néel was well aware of the limitations of (2) but assumed that a better theory would merely yield improved values of g [1].

In spite of frequent reference to the Néel model, there is considerable disagreement about its applicability to 3d metals. Some authors consider band-structure and Néel calculations as complementary rather than competitive [2], [4], [6]. On the other hand, it has been argued that the Néel theory is too simple or incomplete, because g depends on the electronic structure of the atoms [5], [8]-[10].

To answer the question why and to what extent Néel's theory is compatible with band-structure calculations we will use a real-space approach. A particular problem is how many atomic neighbors need to be considered to explain itinerant anisotropy.

II. Single-Ion Anisotropy

The crystal-field splitting of atomic levels gives rise to single-ion anisotropy [9], [11]-[14], which is generally compatible with the Néel model. For example, the semiquantitative screened-charge model [13], [14], which describes rare-earth ions in a screening gas of conduction electrons, yields

$$g = -n_2\frac{eQ}{4\pi\varepsilon_0}\frac{e^{-qR}}{R^3}\left(1 + qR + \frac{1}{3}q^2R^2\right) \qquad (3)$$

Here $n_2 = \alpha_J\langle r^2\rangle_{4f}(2J^2 - J)$ is the electrostatic quadrupole moment of the Hund's-rules rare-earth ions [11], $q \approx 2.3$ Å^{-1} [15] is an inverse Thomas-Fermi screening length, and Q is the charge of the magnetic or *nonmagnetic* crystal-field creating atom.

A minor single-ion effect in 3d metals is that magnetic and nonmagnetic atomic neighbors shift the centers of gravity of the subband densities of states (DOS). The subband shifts are given by $V_{\mu\mu} = \langle\mu|V|\mu\rangle$, where $|\mu\rangle$ is the corresponding atomic orbital and V is the anisotropic crystal-field potential. For example, the lowest-order uniaxial expression $V(\mathbf{r}) = A_2^0\,(3z^2\text{-}r^2)$ [11] yields the energy shifts -2Δ (a_{1g}: z^2), $-\Delta$ (e_{1g}: yz and zx) and 2Δ (e_{2g}: xy and $x^2\text{-}y^2$). Due to electronic repulsion, crystal-field charges tend to be negative [13], so that $\Delta > 0$, and a typical order of magnitude, estimated from Ni band-structure calculations [16], is $\Delta = 0.3$ eV. Similar arguments apply to crystal fields in Co/Cu and Co/Pd multilayers [9], [10] as well as to interface interactions parametrized by constants L_m [3]. Note, however, that the leading contribution to the metallic 3d level splitting is interatomic hopping rather than single-ion crystal-field splitting.

Manuscript received October 16, 1997.

III. Moments Description

The starting point is the tight-binding Hamiltonian

$$E_{\mu\mu'}(\mathbf{k}) = \Sigma_i T_{\mu\mu'}(\mathbf{R}_i)\, e^{i\mathbf{k}\cdot\mathbf{R}_i} + V_{\mu\mu'} + S_{\mu\mu'} \quad (4)$$

where $S_{\mu\mu'} = \lambda\langle\phi_\mu|\hat{\mathbf{s}}.\mathbf{l}|\phi_{\mu'}\rangle$ describes the spin-orbit interaction ($\lambda \approx 50$ meV) [10] and the $T_{\mu\mu'}(\mathbf{R})$ are known functions of the fundamental hopping integrals $V_{dd\sigma}$, $V_{dd\pi}$, and $V_{dd\delta}$ [17].

In the simple case of interacting xy and x^2-y^2 $\downarrow$ orbitals one has to diagonalize the matrix

$$E_{\mu\mu'} = \begin{pmatrix} A & 0 \\ 0 & -A \end{pmatrix} + 2\lambda \cos\theta \begin{pmatrix} 0 & -i \\ i & 0 \end{pmatrix} \quad (5)$$

where θ is the angle between the film normal and the magnetization and $A(\mathbf{k})$ contains both hopping and crystal-field interactions. Equation (5) yields the energy levels $\pm[A^2 + 4\lambda^2\cos^2\theta]^{1/2}$ and, for $\lambda \ll A$, anisotropy energies of order $\lambda^2\cos^2\theta/A$. From this equation we see that subband anisotropies decrease with increasing subband width $W \sim 2A$. However, the sign of the anisotropy contribution depends on the matrix elements $S_{\mu\mu'}$. Typical band-structure anisotropy calculations (see e.g [10] and references therein) are based on perturbation theory with respect to $S_{\mu\mu'}$, but in that approach the real-space meaning of anisotropy is hidden in numerical part of the calculation.

A systematic real-space description starts from the *moments theorem* [18], [19], which deals with the m-th moments $\mu_i^{(m)} = \int (E - \mathcal{H}_{ii})^m D_i(E)\, dE$ of the local densities of states $D_i(E)$ of an $N \times N$ matrix Hamiltonian $\mathcal{H}_{ik}$ [20]. It states that exact moments are obtained by counting closed real-space m-hop loops, even if $m \ll N$. Fixing the zero-point energy by putting $\mathcal{H}_{ii} = 0$ yields $\mu_i^{(2)} = \Sigma_{j\neq i}\, \mathcal{H}_{ij}\, \mathcal{H}_{ji}$ and

$$\mu_i^{(3)} = \Sigma_{j\neq i,k\neq i}\, \mathcal{H}_{ij}\, \mathcal{H}_{jk}\, \mathcal{H}_{ki} \quad (6)$$

In the context of magnetic anisotropy, the indices are *multi-indices* denoting not only the atomic site but also the spin and the magnetic quantum number of d electrons [21]. In particular, due to spin-orbit coupling the subband moments (and the total energies for a given number n of 3d electrons) depend on the magnetization direction.

Straightforward calculation yields the second moment [22]

$$\mu^{(2)}_n = \Sigma_{jn'} T^2_{nn'}(\mathbf{R}_j) \quad (7)$$

whose graphical meaning is shown in Fig. 1(a). The third moment is

$$\mu^{(3)}_n = \Sigma_{jn} V_j T^2_{nn'}(\mathbf{R}_j) - \Delta E\, c_n \lambda^2 \sin^2\theta + \delta_n \quad (8)$$

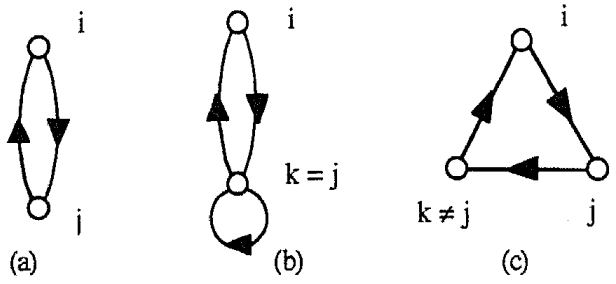

Fig. 1. Elementary hopping loops.

where V_j is the average 3d energy on the site j and $\Delta E = \mathrm{Im}/\mu_B$ is the Stoner exchange splitting ($I \approx 1$ eV). When the magnetization is confined to the x-z plane then $c_{xy} = c_{x^2-y^2} = -3/4$, $c_{zx} = 0$, and $c_{yz} = c_{z^2} = 3/4$. The term δ_n describes real-space configurations of the type Fig. 1(c) and goes beyond the Néel model (see below).

Since the $\mu^{(2)}_n$ are independent of λ, there is *no second-moment anisotropy*. Lowest-order itinerant anisotropy arises from the ΔE term in Eq. (8), which gives rise to a small θ-dependent DOS asymmetry. Now we approximate the true subband densities of states by rectangles whose widths $W_n = (12\mu^{(2)}_n)^{1/2}$ are obtained from Eq. (7) and obtain [22] analytic anisotropy expressions. In ultrathin films and at surfaces, the pronounced in-plane interatomic hopping means that the xy and x^2-y^2 subbands are wider than the z^2, yz, and zx subbands. For a (001) monolayer (square lattice), the anisotropy Fig. 2 is obtained. The anisotropy is of order λ^2/W, but its exact magnitude (the K_1 scale in Fig. 2) and, to a minor extent, the positions of the zeros reflects the number of nearest neighbors, their coordination, and the interatomic distances.

In agreement with numerical band-structure cal-

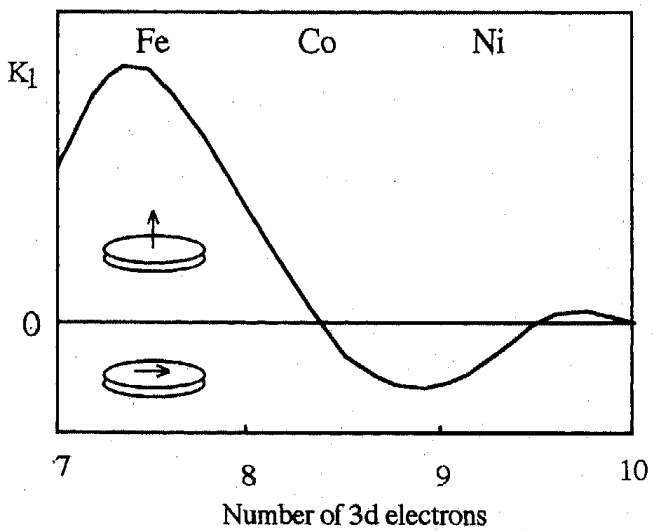

Fig. 2. Schematic band-filling dependence of the anisotropy. As a guide for the eyes, approximate atomic meanings of the band filling are shown at the top of the figure.

culations and experimental data [5], [10], [23], [24], the anisotropy oscillates as a function of n, but due to the restriction to pair interactions the n resolution is poor. Furthermore, as mentioned the curves show some dependence on the film or surface structure.

Note that the present solid-state moments approach is related to the quasimolecular diatomic pair model [23]. The moments approach works best for small exchange splittings but requires the inclusion of higher-order graphs to reproduce the diatomic pair limit of strong exchange splitting.

IV. Discussion and Conclusions

Since the number of magnetic and nonmagnetic neighbours and their spatial coordinations are contained in (7), the Néel model is able to distinguish between monolayers, surfaces, bulk magnets and clusters. Ultimately, it yields an expansion of the magnetic energy into spherical harmonics and gives a proper account of the symmetry of ordered and disordered surfaces. For example, in disordered magnets it yields not only $\sin 2\phi$ contributions, as it is well-known for surfaces vicinal to fcc (001), but also $\sin \phi$ contributions.

However, the pair model is unable to reproduce band-structure details which involve more than two atoms. For example, the real-space *triangle* term

$$\delta_n = \Sigma_{jkn'n''} T_{nn'}(\mathbf{R}_j) T_{n'n''}(\mathbf{R}_k - \mathbf{R}_j) T_{n''n}(\mathbf{R}_k) \quad (10)$$

shown in Fig. 1(c) is nonzero in fcc (111) monolayers but zero in fcc (001) monolayers. Higher-order terms such as δ_n are necessary to tune the Fermi level when it lies between two quasi-degenerate states ($A \leq \lambda$). Similarly, the V_j term in (8) is nonzero for nonmagnetic or chemically different magnetic neighbors (Fig. 1(b)) [19]. In general, the inclusion of higher-order terms improve the resolution of the $K_1(n)$ curve and may even yield additional zeros.

Since compressive surface relaxations and Poisson contractions of films can be interpreted as tetragonally distorted $c/a < 1$ environments, as compared to cubic structures ($c/a = 1$) and monolayers ($c/a = \infty$), we expect that $c/a < 1$ configurations and monolayers yield opposite anisotropy contributions. The reason is that intraplane and interplane overlaps dominate for $c/a > 1$ and $c/a < 1$, respectively.

In conclusion, we have shown that the Néel model goes far beyond the original assumption of quasi-dipolar pair interactions between localized atoms. This refers not only to rare-earth ions but also to 3d metals, where Néel-type contributions are explained in terms of third-moment atomic-pair contributions. This means that the Néel theory contains the metallic band structure and the influence of interface atoms on a rudimentary level.

Acknowledgment

The author is grateful to J. Cullen, W. Hübner, J. Kirschner, M. Richter, and D. Sander for interesting discussions.

References

[1] L. Néel, *J. Phys. Rad.*, vol. 15, p. 376, 1954).
[2] U. Gradmann, in: *Handbook of Magnetic Materials*, vol. 7, K. H. J. Buschow, Ed., Elsevier: Amsterdam 1993, pp. 1-95.
[3] R. H. Victora and J. M. McLaren, *Phys. Rev. B*, vol. 47, 1993, p. 11583.
[4] P. Bruno, *J. Phys. F: Met. Phys.*, vol. 18, 1988, p. 1291.
[5] M. T. Johnson, P. J. H. Bloemen, F. J. A. den Broeder, and J. J. de Vries, *Rep. Prog. Phys.*, vol. 59, 1996, pp. 1409-1458.
[6] D. S. Chuang, C. A. Ballentine, and R. C. O'Handley, *Phys. Rev. B*, vol. 49, 1994, p. 15084.
[7] F. Bloch and G. Gentile, *Z. Phys.*, vol. 70, 1931, p. 395.
[8] P. Krams, B. Hillebrands, G. Güntherodt, and H.-P. Oepen, *Phys. Rev. B*, vol. 49, 1994, p. 3633.
[9] D.-Sh. Wang, R.-Q. Wu, and A. J. Freeman, *J. Magn. Magn. Mater.*, vol. 129, 1994, p. 237.
[10] J. A. C. Bland and B. Heinrich, Eds., *Ultrathin Mmagnetic Structures I*, Berlin: Springer, 1994.
[11] M. T. Hutchings, *Solid State Phys.*, vol. 16, 1964, pp. 227-273.
[12] R. Skomski, *IEEE Trans. Magn.*, vol. 32, 1996, pp. 4794-4796.
[13] R. Skomski, *Phil. Mag. B*, vol. 70, 1994, p. 175.
[14] L. Steinbeck, M. Richter, U. Nitzsche, and H. Eschrig, *Phys. Rev. B*, vol. 53, 1996, p. 7111.
[15] S. Wirth, M. Wolf, K.-H. Müller, R. Skomski, S. Brennan, and J. M. D. Coey, *IEEE Trans. Magn.*, vol. 32, 1996, p. 4746.
[16] O. Jepsen, J. Madsen, and O. K. Andersen, *Phys. Rev. B*, vol. 26,1982, pp. 2790-2809.
[17] J. C. Slater and G. F. Koster, *Phys. Rev.*, vol. 94, 1954, p. 1498.
[18] F. Cyrot-Lackmann, J. Phys. Chem. Solids, vol. 29, 1968, p. 1235.
[19] A. P. Sutton, *Electronic Structure of Materials*, University Press: Oxford, 1993.
[20] The first moment is the subband center of gravity, the second moment determines the band width, and higher-order moments reproduce details of the DOS.
[21] V. Heine, W. C. Kok, and C. M. M. Nex, *J. Magn. Magn. Mater.*, vol. 43, 1984, p. 61.
[22] Calculational details will be published elsewhere.
[23] D.-Sh. Wang, R.-Q. Wu, and A. J. Freeman, *Phys. Rev. B*, vol. 47, 1993, pp. 14932-14947.
[24] P. Bruno, *Phys. Rev. B*, vol. 39, 1989, p. 865.